Published for SISSA by Springer

Received: November 19, 2018
Revised: March 9, 2019
Accepted: March 19, 2019
Published: April 1, 2019

Invisible neutrino decays at the MOMENT experiment

Jian Tang,[a] **Tse-Chun Wang**[a] **and Yibing Zhang**[a,b]

[a] *School of Physics, Sun Yat-Sen University,*
No. 135, Xingang Xi Road, Guangzhou, 510275, P.R. China
[b] *School of Mathematical and Physical Sciences, University of Sussex,*
Falmer, Brighton BN1 9RH, U.K.

E-mail: tangjian5@mail.sysu.edu.cn, wangzejun@mail.sysu.edu.cn, yz454@sussex.ac.uk

Abstract: We investigate invisible decays of the third neutrino mass eigenstate in future accelerator neutrino experiments using muon-decay beams such as MuOn-decay MEdium baseline NeuTrino beam experiment (MOMENT). MOMENT has outstanding potential to measure the deficit or excess in the spectra caused by neutrino decays, especially in ν_μ and $\bar{\nu}_\mu$ disappearance channels. Such an experiment will improve the constraints of the neutrino lifetime τ_3. Compared with exclusion limits in the current accelerator neutrino experiments T2K and NOvA under the stable ν assumption, we expect that MOMENT gives the bound of $\tau_3/m_3 \geq 10^{-11}\,\mathrm{s/eV}$ at 3σ, which is better than their recent limits: $\tau_3/m_3 \geq 7 \times 10^{-13}\,\mathrm{s/eV}$ in NOvA and $\tau_3/m_3 \geq 1.41 \times 10^{-12}\,\mathrm{s/eV}$ in T2K. The non-decay scenario is expected to be excluded by MOMENT at a confidence level $> 3\sigma$, if the best fit results in T2K and NOvA are confirmed. We further find that reducing systematic uncertainties is more important than the running time. Finally, we find some impact of τ_3/m_3 on the precision measurement of other oscillation parameters.

Keywords: Beyond Standard Model, Neutrino Physics

ArXiv ePrint: 1811.05623

https://doi.org/10.1007/JHEP04(2019)004

JHEP04(2019)004

Contents

1 Introduction

The oscillation pattern of three-flavour neutrino mixing has been established through solar, atmospheric, accelerator and reactor neutrino experiments [1–4]. In the standard three-flavour paradigm, neutrino oscillations are dominated by two mass-squared splittings (i.e., Δm^2_{31}, Δm^2_{21}) and three mixing angles (i.e. θ_{12}, θ_{13}, θ_{23}) [5]. Up to now, most of the oscillation parameters have been measured well [6], except the Dirac CP phase δ and the neutrino mass ordering (normal mass hierarchy: $\Delta m^2_{31} > 0$; inverted mass hierarchy: $\Delta m^2_{31} < 0$). The precision of measuring θ_{23} is not good enough to discriminate the octant degeneracies with a specific prediction $\theta_{23} = 45°$. All these unknown parameters will be measured in the near future by medium baseline reactor experiments: JUNO [7] and RENO [8], and by the long-baseline accelerator neutrino experiments: T2K [9], NOvA [10], T2HK [9] and DUNE [11]. Recent results from T2K and NOvA incline to a normal mass hierarchy and indicate a hint of $\delta \approx 270°$ [12, 13] only at a low confidence level. Therefore, we are looking forward to data provided by the next-generation experiments to attain a compelling conclusion. Since we are entering an era of precision measurements, it is natural to expect near future neutrino oscillation experiments to search for new physics beyond three-generation neutrino oscillations including sterile neutrinos, neutrino decays and non-standard neutrino interactions, and so on.

Neutrino decays are classified into invisible and visible scenarios. Several models depend on whether neutrinos are Majorana or Dirac particles [14–21]. If the final states of neutrino decays are unobservable to the detector, those decays are called invisible decays [21]. There are decay models $\nu_j \to \nu_4 + J$ for Majorana neutrinos [16–18], where J denotes a Majoron. Another class of models assumes that neutrinos are Dirac particles

JHEP04(2019)004

and the coupling which gives rise to neutrino decay: $\nu_i \to \bar{\nu}_{jR} + \chi$, where χ is a light iso-singlet scalar and ν_{iR} is a right-handed fermion [14, 15]. In the visible decay scenario, decay products can be detected by the detector. Several decay patterns like $\nu_j \to \bar{\nu}_i(\nu_i) + J$ have been put forward [19–21].

The ν_2 decay in the invisible channel has been constrained well from solar neutrino oscillation data, which gives the bound $\tau_2/m_2 > 7.2 \times 10^{-4}\,\mathrm{s/eV}$ at 90% C.L. [22, 23]. There are proposals to constrain the neutrino decays life time with the help of solar neutrino oscillations detected by the liquid Xenon detector [24]. Atmospheric and long-baseline neutrino experiments set a bound on the decay lifetime for ν_3, such as $\tau_3/m_3 > 2.9 \times 10^{-10}\,\mathrm{s/eV}$ at 90% C.L. [25]. Recently, invisible neutrino decays have been used to explain the IceCube track and cascade tension [26]. A sensitivity study of invisible neutrino decays has been conducted for KM3NeT-ORCA [27]. MINOS and T2K experiments have constrained the neutrino decay lifetime as $\tau_3/m_3 > 2.8 \times 10^{-12}\,\mathrm{s/eV}$ at 90% confidence level [28]. Recently a combined analysis of NOvA and T2K data points to a result of $\tau_3/m_3 > 1.5 \times 10^{-12}\,\mathrm{s/eV}$ along with the constraints by individual experiments: $\tau_3/m_3 \geq 7 \times 10^{-13}\,\mathrm{s/eV}$ in NOvA and $\tau_3/m_3 \geq 1.41 \times 10^{-12}\,\mathrm{s/eV}$ in T2K [32]. The expected bounds for JUNO [29], INO [30] and DUNE [31] can reach $\tau_3/m_3 > 7.5\ (5.5) \times 10^{-11}\,\mathrm{s/eV}$ at 95% (99%) C.L., $\tau_3/m_3 > 1.51 \times 10^{-10}\,\mathrm{s/eV}$ at 90% C.L. and $\tau_3/m_3 > 4.5 \times 10^{-11}\,\mathrm{s/eV}$ at 90% C.L., respectively.

Some studies focus on visible decays. For example, a study shows that DUNE will be sensitive to the level of $\tau_3/m_3 < 1.95\text{–}2.6 \times 10^{-10}\,\mathrm{s/eV}$ at $> 90\%$ C.L., and the combination of MINOS and T2K gives the bound $\tau_3/m_3 > 1.5 \times 10^{-11}\,\mathrm{s/eV}$ at a confidence level $> 90\%$ [33]. As visible neutrino decays offer clear signals in the detector, it is even more difficult to constrain invisible decays than in the visible case. Because the bound for the invisible neutrino decay like τ_3 is much worse than τ_2, it is valuable to exploit the measurement potential of invisible ν_3 decays in next generation neutrino oscillation experiments. We further point out that in addition to searching for them in neutrino oscillation experiments, we can also find evidence for neutrino decays in astrophysical observations due to their influence on the formation of cosmological perturbations [34, 35].

Apart from superbeam neutrino experiments, it is desirable to study new physics at muon-decay accelerator neutrino experiments. In such experiments, neutrinos come from a three-body decay process, avoiding intrinsic electron-flavor neutrino contaminations in the reconstructed oscillation signals from the source. Apart from such an advantage, MOMENT [36] is likely to use a Gd-dopped water cherenkov detector capable of detecting multiple channels, which have been demonstrated to have excellent properties to study new physics, including NSIs [37–39] and sterile neutrinos [40–43]. In the current work, we focus on the constraints of neutrino decays into invisible products, and demonstrate how the ν_3 decay would affect precision measurements of standard neutrino mixing parameters.

This paper is organized as follows: we describe the basic framework for neutrino oscillations with invisible neutrino decays taken into account and study the oscillation probabilities for the MOMENT experiment in section 2. Implementations and simulation details are given in section 3, and in the same section, we also investigate the impact of neutrino decays on the spectra of MOMENT. In section 4, we present simulation results, mainly

JHEP04(2019)004

focusing on the constraints on the ν_3 lifetime, compare it to the reach of current experiments, and investigate the impacts of the total running time, systematic uncertainty and energy resolution on this measurement, with the study on the expected exclusion level to the stable-neutrino assumption and their impacts on precision measurements of θ_{23} and Δm^2_{31}. Finally, we summarize in section 5.

2 Neutrino oscillations with invisible neutrino decays

The latest results from MiniBooNE have an excess for reconstructed oscillation spectra [44], suggesting the existence of sterile neutrinos. We assume that the neutrino decay products are sterile neutrinos. In addition, we consider that the third mass eigenstate decays in the following channel: $\nu_3 \to \nu_4 + J$, where normal mass hierarchy and a light sterile neutrino are considered (i.e. $m_3 > m_2 > m_1 > m_4$). The connection between flavour eigenstates and mass eigenstates can be given as:

$$\begin{pmatrix} \nu_\alpha \\ \nu_s \end{pmatrix} = \begin{pmatrix} U & 0 \\ 0 & 1 \end{pmatrix} \begin{pmatrix} \nu_i \\ \nu_4 \end{pmatrix} \tag{2.1}$$

The Hamitonian of neutrino propagation in matter can be written as:

$$H = U \left\{ \frac{1}{2E} \begin{pmatrix} 0 & 0 & 0 \\ 0 & \Delta m^2_{21} & 0 \\ 0 & 0 & \Delta m^2_{31} \end{pmatrix} - i \frac{m_3}{2E\tau_3} \begin{pmatrix} 0 & 0 & 0 \\ 0 & 0 & 0 \\ 0 & 0 & 1 \end{pmatrix} \right\} U^\dagger + \begin{pmatrix} 2\sqrt{2}G_F N_e E & 0 & 0 \\ 0 & 0 & 0 \\ 0 & 0 & 0 \end{pmatrix}, \tag{2.2}$$

where U is the PMNS mixing matrix [45, 46], G_F is the Fermi coupling constant, N_e is the electron density, E is the neutrino energy and τ_3 is the lifetime of ν_3. Obviously, the probabilities for neutrino and antineutrino modes remain invariant with a replacement of $\delta \to -\delta$ and $N_e \to -N_e$, i.e. $P_{\nu_\alpha \to \nu_\beta}(E, L; \delta, N_e) = P_{\bar{\nu}_\alpha \to \bar{\nu}_\beta}(E, L; -\delta, -N_e)$. Then we can calculate the numerical oscillation probabilities by diagonalizing the Hamitonian matrix. The diagonalization method can be found in ref. [47]. Our numerical tool to evaluate the probabilities with neutrino decays has been checked by comparing our result with those shown in ref. [31]. To cross check validity of our codes, we have reproduced the invisible-neutrino-decay result from ref. [32], highlighting the current measurement at T2K and NOvA. The probability for the antineutrino mode has been cross checked by a comparison with the neutrino mode taking the opposite sign of δ and N_e.

The probabilities with ν decays in vacuum are given as follows,

$$\begin{aligned} P_{\nu_\alpha \to \nu_\beta}(E, L; \delta) = \Big| & U_{\alpha 1}(\delta) U^*_{\beta 1}(\delta) + U_{\alpha 2}(\delta) U^*_{\beta 2}(\delta) \exp\left(-i \frac{\Delta m^2_{21}}{2E}\right) \\ & + U_{\alpha 3}(\delta) U^*_{\beta 3}(\delta) \exp\left(-\Gamma_3 L\right) \exp\left(-i \frac{\Delta m^2_{31}}{2E}\right) \Big|^2 . \end{aligned} \tag{2.3}$$

JHEP04(2019)004

This can be further expanded as

$$
\begin{aligned}
P_{\nu_\alpha\to\nu_\beta}(E,L;\delta) = {} & U^*_{\alpha1}(\delta)U_{\beta1}(\delta)U_{\alpha1}(\delta)U^*_{\beta1}(\delta) + U^*_{\alpha2}(\delta)U_{\beta2}(\delta)U_{\alpha2}(\delta)U^*_{\beta2}(\delta) \\
& + U^*_{\alpha3}(\delta)U_{\beta3}(\delta)U_{\alpha3}(\delta)U^*_{\beta3}(\delta)\exp(-2\Gamma_3 L) \\
& + \mathrm{Re}\left[U^*_{\alpha2}(\delta)U_{\beta2}(\delta)U_{\alpha1}(\delta)U^*_{\beta1}(\delta)\right]\cos\left(\frac{\Delta m^2_{21}L}{2E}\right) \\
& + \mathrm{Im}\left[U^*_{\alpha2}(\delta)U_{\beta2}(\delta)U_{\alpha1}(\delta)U^*_{\beta1}(\delta)\right]\sin\left(\frac{\Delta m^2_{21}L}{2E}\right) \\
& + \mathrm{Re}\left[U^*_{\alpha3}(\delta)U_{\beta3}(\delta)U_{\alpha1}(\delta)U^*_{\beta1}(\delta)\right]\exp(-\Gamma_3 L)\cos\left(\frac{\Delta m^2_{31}L}{2E}\right) \\
& + \mathrm{Im}\left[U^*_{\alpha3}(\delta)U_{\beta3}(\delta)U_{\alpha1}(\delta)U^*_{\beta1}(\delta)\right]\exp(-\Gamma_3 L)\sin\left(\frac{\Delta m^2_{31}L}{2E}\right) \\
& + \mathrm{Re}\left[U^*_{\alpha3}(\delta)U_{\beta3}(\delta)U_{\alpha2}(\delta)U^*_{\beta2}(\delta)\right]\exp(-\Gamma_3 L)\cos\left(\frac{\Delta m^2_{32}L}{2E}\right) \\
& + \mathrm{Im}\left[U^*_{\alpha3}(\delta)U_{\beta3}(\delta)U_{\alpha2}(\delta)U^*_{\beta2}(\delta)\right]\exp(-\Gamma_3 L)\sin\left(\frac{\Delta m^2_{32}L}{2E}\right),
\end{aligned}
\tag{2.4}
$$

where $\Gamma_3 \equiv \frac{m_3}{2E\tau_3}$. For the antineutrino mode, δ is replaced by $-\delta$. Eq. (2.4) is consistent with eq. (A.2) in [29]. It is clear that through the final 4 terms of eq. (2.4) neutrino decays provide damping effects to the Δm^2_{31} and Δm^2_{32} oscillations. Further, the decays also cause an overall decrease via the third term. Both effects can be seen in the following.

We show the probability for four channels $\nu_\mu \to \nu_\mu$ (upper-left), $\nu_e \to \nu_e$ (upper-right), $\nu_e \to \nu_\mu$ (lower-left), and $\nu_\mu \to \nu_e$ (lower-right) of MOMENT in figure 1 (those for the antineutrino mode are in figure 2). For the case with neutrino decays, we consider those within $10^{-12}\,\mathrm{s/eV} < \tau_3/m_3 < 10^{-9}\,\mathrm{s/eV}$ (red band), and compare it with that for the case without neutrino decays (black curve). As we can see, the case with $\tau_3/m_3 = 10^{-9}\,\mathrm{s/eV}$ is overlapping with the curves for the case without neutrino decays. For the other extreme case $\tau_3/m_3 = 10^{-12}\,\mathrm{s/eV}$, the probabilities are far from the black curves. In the following, we compare the case for $\tau_3/m_3 = 10^{-12}\,\mathrm{s/eV}$ and that without neutrino decays. Except for the minima, in the $\nu_\mu \to \nu_\mu$ channel, we see significant deficits. Around the minima, we notice the fact that the probability with neutrino decays goes above or below the curve corresponding to the stable-neutrino assumption. This is because the suppression term dominates the damping ones. Moving to the smaller τ_3/m_3, $U^*_{\alpha3}(\delta)U_{\beta3}(\delta)U_{\alpha3}(\delta)U^*_{\beta3}(\delta)\exp(-2\Gamma_3 L)$ gets smaller earlier than the damping terms because of the factor of 2 in the exponential. When this effect does not dominate the damping one, the probability goes upper around the minima. The competition between these two effects is also seen in the $\nu_e \to \nu_\mu$ and $\bar{\nu}_\mu \to \bar{\nu}_e$ channels. Therefore, the maxima in the ν_μ and $\bar{\nu}_\mu$ disappearance channels could be useful for measuring the effect of neutrino decays. The damping effect in ν_e and $\bar{\nu}_e$ disappearance channels is obvious. Further, we see an overall decrease in $P(\nu_e \to \nu_\mu)$, while the impact of neutrino decays on $P(\nu_\mu \to \nu_e)$ is similar to that for e disappearance channels — it smoothens out the probability (damping effects). The amount of impact in $P(\nu_\mu \to \nu_e)$ is similar to that in $P(\nu_e \to \nu_\mu)$. We see similar results for the antineutrino mode, except for the opposite pattern in the appearance channels: $P(\nu_\mu \to \nu_e) \sim P(\bar{\nu}_e \to \bar{\nu}_\mu)$ and

JHEP04(2019)004

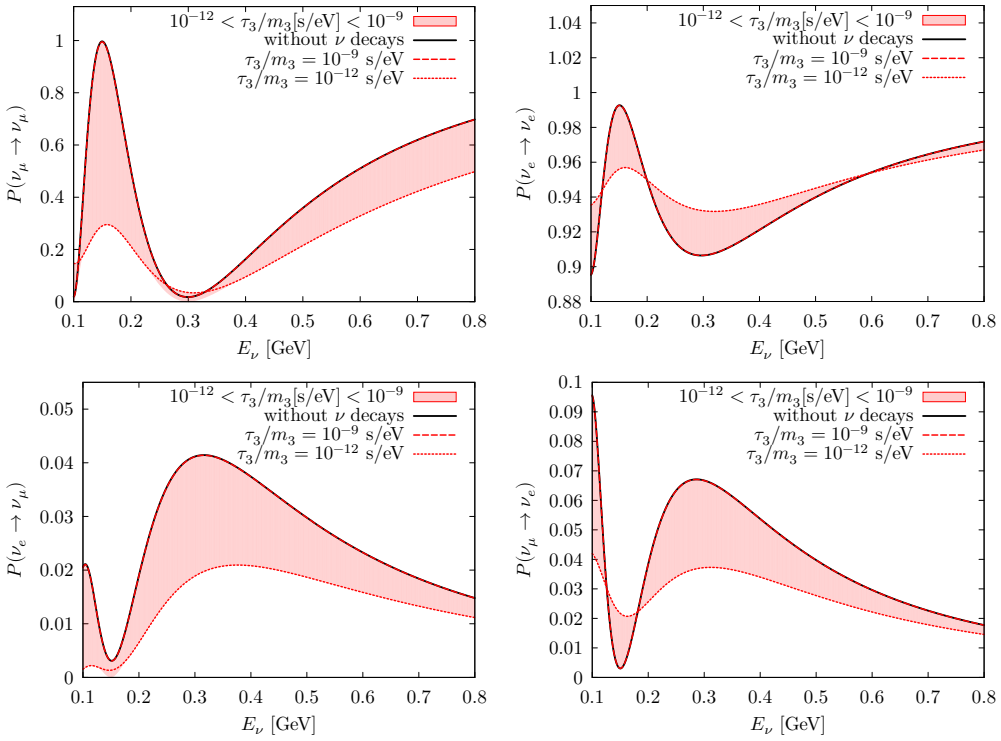

Figure 1. The oscillation probabilities within $10^{-12}\,\mathrm{s/eV} < \tau_3/m_3 < 10^{-9}\,\mathrm{s/eV}$ (red band) for MOMENT. We especially present the probability with $\tau_3/m_3 = 10^{-12}\,\mathrm{s/eV}$ (red-dotted curve), $= 10^{-9}\,\mathrm{s/eV}$ (red-dashed curve) and $= \infty$ (black curve). Four channels are shown: $\nu_\mu \to \nu_\mu$ (upper-left), $\nu_e \to \nu_e$ (upper-right), $\nu_e \to \nu_\mu$ (right-left), and $\nu_\mu \to \nu_e$ (lower-right). The following oscillation parameters are used: θ_{12}=33.8°, $\theta_{13} = 8.61°$, $\theta_{23} = 49.6°$, $\Delta m^2_{21} = 7.39 \times 10^{-5}\,\mathrm{eV}^2$, $\Delta m^2_{31} = 2.52 \times 10^{-3}\,\mathrm{eV}^2$, and $\delta = 270°$.

$P(\nu_e \to \nu_\mu) \sim P(\bar{\nu}_\mu \to \bar{\nu}_e)$. Based on the size of variations, we reach the conclusion that the μ-flavour disappearance channel is the more important than the other channels in the measurement of τ_3/m_3.

3 Simulated spectra with neutrino decays in MOMENT

The simulation details for MOMENT are shown in table 1 with the neutrino sources, detector descriptions and running time [48, 49]. MOMENT, as a medium muon decay accelerator neutrino experiment, is proposed as a future experiment to measure the leptonic CP-violating phase. The neutrino fluxes are kindly offered by the MOMENT working group [36]. Here we utilize eight oscillation channels: $\nu_e \to \nu_e$, $\nu_e \to \nu_\mu$, $\nu_\mu \to \nu_e$, $\nu_\mu \to \nu_\mu$ and their CP-conjugate partners. We have to consider flavour and charge identifications to distinguish secondary particles by means of an advanced neutrino detector. The charged-current interactions are used to identify neutrino signals: $\nu_e + n \to p + e^-$, $\bar{\nu}_\mu + p \to n + \mu^+$, $\bar{\nu}_e + p \to n + e^+$, and $\nu_\mu + n \to p + \mu^-$. We consider the new technology using Gd-dopped water to separate both Cherenkov and coincident signals from the capture of thermal neutrons [50, 51]. The major backgrounds are mostly from the atmospheric neutrinos,

JHEP04(2019)004

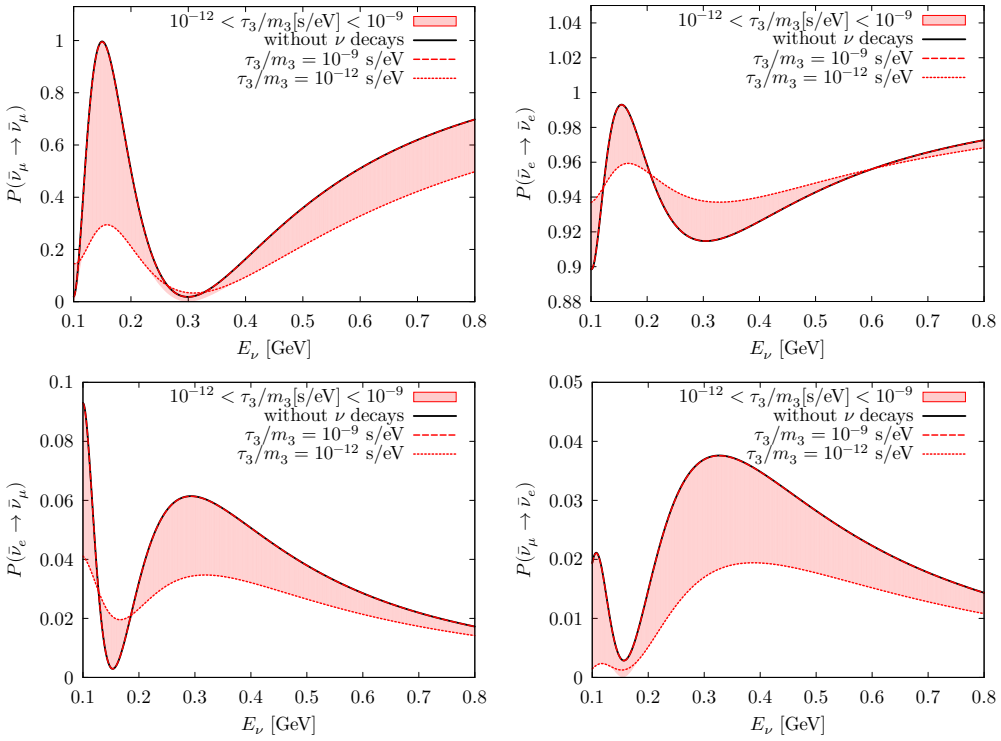

Figure 2. The oscillation probabilities within $10^{-12}\,\mathrm{s/eV} < \tau_3/m_3 < 10^{-9}\,\mathrm{s/eV}$ (red band) for MOMENT. We especially present the probability with $\tau_3/m_3 = 10^{-12}\,\mathrm{s/eV}$ (red-dotted curve), $= 10^{-9}\,\mathrm{s/eV}$ (red-dashed curve) and $= \infty$ (black curve). Four channels are considered: $\bar{\nu}_\mu \to \bar{\nu}_\mu$ (upper-left), $\bar{\nu}_e \to \bar{\nu}_e$ (upper-right), $\bar{\nu}_e \to \bar{\nu}_\mu$ (right-left), and $\bar{\nu}_\mu \to \bar{\nu}_e$ (lower-right). The following oscillation parameters are used: θ_{12}=33.8°, θ_{13}=8.61°, θ_{23}=49.6°, Δm^2_{21}=7.39×10^{-5} eV^2, Δm^2_{31}=2.52×10^{-3} eV^2, and $\delta = 270°$.

neutral current backgrounds and charge mis-identifications. They can be largely suppressed by the beam direction and proper modelling of background spectra within the beam-off period, which is to be extensively studied in detector simulations. In section 4.2, we will compare the physics capabilities under different assumptions, including a change of total running time.

Our simulation is carried out with the help of a GLoBES package [52, 53]. The following central values and their uncertainties of the standard neutrino oscillation parameters are taken from the latest NuFit4.0 results [6]: θ_{12}=33.82° (2.3%), θ_{13}=8.61° (1.8%), θ_{23}=49.6° (5.8%), Δm^2_{21}=7.39×10^{-5} eV^2 (2.4%), Δm^2_{31}=2.525×10^{-3} eV^2 (1.6%), $\delta = 270°$ (no prior applied). In the following, we will assume the normal mass hierarchy, i.e. $\Delta m^2_{31} > 0$.

We present the event spectra for each channels of MOMENT in figures 3 and 4. Similar to figures 1 and 2, the spectra for the case with $\tau_3/m_3 = 10^{-9}\,\mathrm{s/eV}$ exactly overlap the spectra for the case without neutrino decays. The extreme case $\tau_3/m_3 = 10^{-12}\,\mathrm{s/eV}$ is far from the black spectra, which are predicted assuming stable neutrinos. In the following, we focus on a comparison of results given different assumptions. We observe the advantage of the lower energy events, as the larger deviations from the spectra for the case without neutrino decays appear in the lower-energy bins. Comparing all panels in figures 3 and 4, we

JHEP04(2019)004

Experiments	MOMENT
Fiducial mass	Gd-dopped Water cherenkov(500 kton)
Channels	$\nu_e(\bar{\nu}_e) \to \nu_e(\bar{\nu}_e)$, $\nu_\mu(\bar{\nu}_\mu) \to \nu_\mu(\bar{\nu}_\mu)$, $\nu_e(\bar{\nu}_e) \to \nu_\mu(\bar{\nu}_\mu)$, $\nu_\mu(\bar{\nu}_\mu) \to \nu_e(\bar{\nu}_e)$
Energy resolution	$12\%/E$
Runtime	μ^- mode 5 yrs+ μ^+ mode 5 yrs
Baseline	150 km
Energy range	100 MeV to 800 MeV
Normalization (error on signal)	appearance channels: 2.5% disappearance channels: 5%
Normalization (error on background)	Neutral current, Atmospheric neutrinos Charge misidentification

Table 1. Assumptions for the source, detector and running time for MOMENT in the simulation.

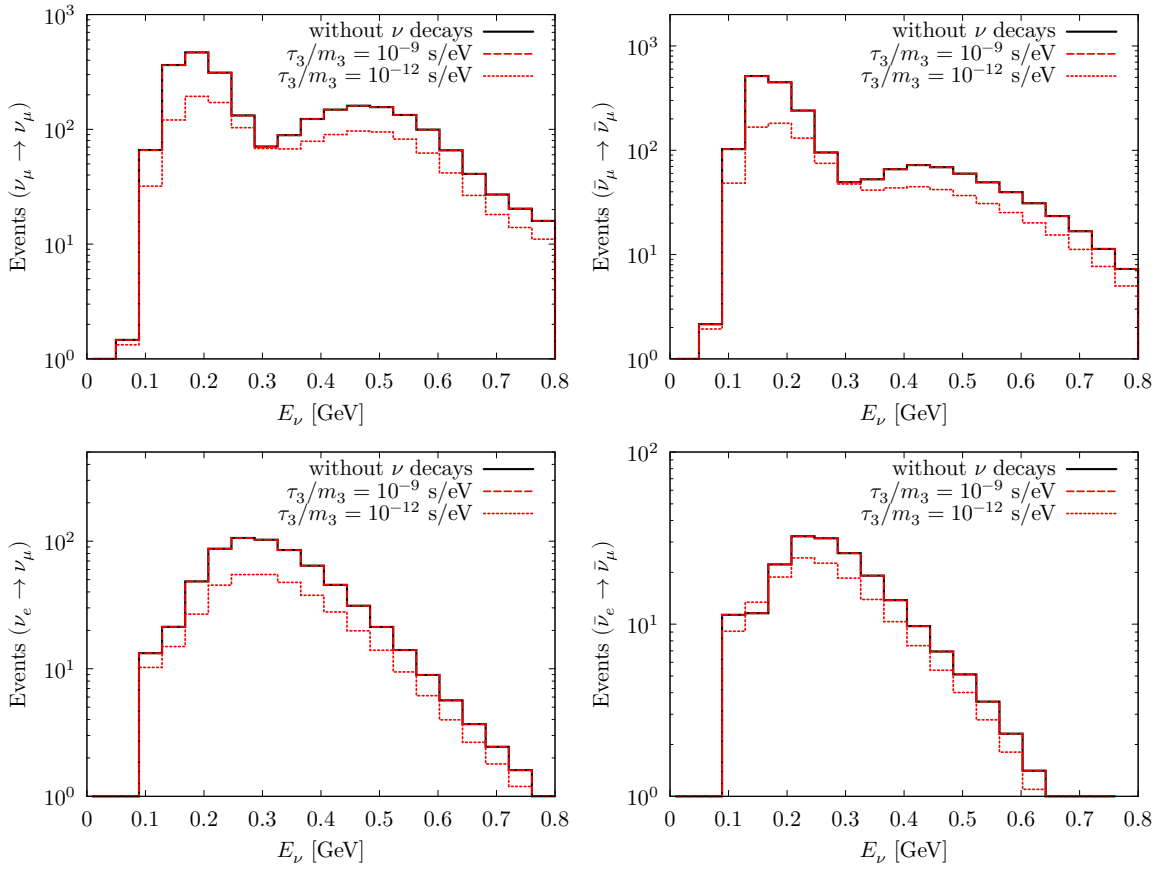

Figure 3. The spectra with $\tau_3/m_3 = 10^{-12}$ s/eV (red-dotted) and $= 10^{-9}$ s/eV (red-dashed) and under the standard model (black) for MOMENT. Four channels are considered: $\nu_\mu \to \nu_\mu$ (upper-left), $\bar{\nu}_\mu \to \bar{\nu}_\mu$ (upper-right), $\nu_e \to \nu_\mu$ (right-left), and $\bar{\nu}_e \to \bar{\nu}_\mu$ (lower-right). The oscillation baseline is set at 150 km.

JHEP04(2019)004

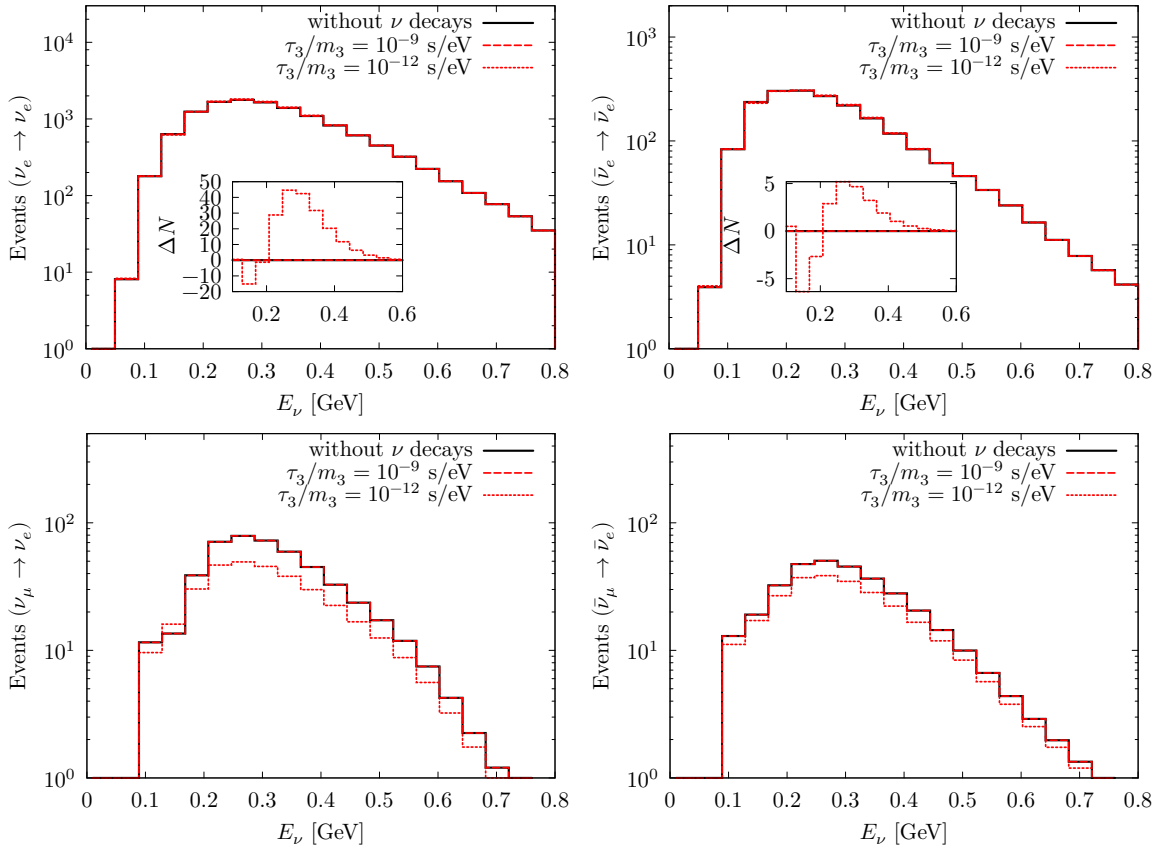

Figure 4. The spectra with $\tau_3/m_3 = 10^{-12}$ s/eV (red-dotted) and $= 10^{-9}$ s/eV (red-dashed) and under the standard model (black) for MOMENT. Four channels are considered: $\nu_e \to \nu_e$ (upper-left), $\bar{\nu}_e \to \bar{\nu}_e$ (upper-right), $\nu_\mu \to \nu_e$ (right-left), and $\bar{\nu}_\mu \to \bar{\nu}_e$ (lower-right). The oscillation baseline is set at 150 km. For clearness, in the result for the ν_e and $\bar{\nu}_e$ disappearance channels, we define ΔN as a difference between event rates with and without neutrino decays in each energy bin.

are reminded of the conclusion from section 2 that the muon-flavour disappearance channels are the most important ones for the measurement of τ_3/m_3, as the larger deviations from the black spectra are observed. In ν_μ and $\bar{\nu}_\mu$ disappearance channels shown in figure 3, we see both suppression and damping effects. The event rate decreases all the way in energy because of neutrino decays. However, the degree of deficit becomes larger around the maximum, while it gets smaller at the minimum. The change in these ν_μ and $\bar{\nu}_\mu$ disappearance channels can be a few hundred events per bin, and much larger than those in the other six channels, in which the deficit is a few tens of events per bin. The overall decrease is also seen in $\nu_e \to \nu_\mu$ and $\bar{\nu}_\mu \to \bar{\nu}_e$ channels. However, the number of events decreases in the lower energy bin but increases in the higher energy bin because of neutrino decays in the ν_e and $\bar{\nu}_e$ disappearance channels. We see a reduction of event rates in most energy bins in $\bar{\nu}_e \to \bar{\nu}_\mu$, $\nu_\mu \to \nu_e$, $\bar{\nu}_e \to \bar{\nu}_\mu$ and $\bar{\nu}_\mu \to \bar{\nu}_e$, as shown in the lower panels of figures 3 and 4.

To sum up, it is clear that when we turn on neutrino decays with $\tau_3/m_3 = 10^{-12}$ s/eV, a distinct difference between the cases with and without decays can be easily measured

JHEP04(2019)004

by MOMENT. Invisible decays can wash out the extreme of neutrino oscillations. Therefore, the focus on the maximum or minimum can help us to detect the effect of neutrino decays. Furthermore, the differences in ν_μ and $\bar{\nu}_\mu$ disappearance channels are larger than the other six channels. This implies that the $\nu_\mu \to \nu_\mu$ and $\bar{\nu}_\mu \to \bar{\nu}_\mu$ channels will play an important role in the analysis. This could affect the precision measurement of neutrino mixing parameters such as θ_{23} and Δm^2_{31} which are mostly involved in these channels. As a result, the other channels could help with a clarification of this bias induced by neutrino decays. We eventually come up with the conclusion that MOMENT is expected to have high-level sensitivities to the lifetime of ν_3 since they have multiple channels, and this exactly demonstrates the advantage of Gd-dopped water Cherenkov technology.

4 Results

Based on simulated event spectra with/without neutrino decays, we investigate the precision measurement on τ_3/m_3 of MOMENT, and compare it with the reach by the current experiments. We also study the expected exclusion level to the stable neutrino hypothesis ($\tau_3/m_3 = \infty$) assuming various true values of τ_3/m_3. We further present our results on the impact of statistical error, systematic uncertainty and energy resolution. Finally, we study the contours at 3σ on the $\theta_{23} - \tau_3/m_3$, $\Delta m^2_{31} - \tau_3/m_3$ and $\theta_{23} - \Delta m^2_{31}$ planes.

4.1 Bound on the lifetime of ν_3

In figure 5, we show the constraint on τ_3/m_3 for four different true values: $\tau_3/m_3 = \infty$ (black solid), 10^{-11} (green dashed-dotted), 5.01×10^{-12} (blue short-dashed), and 3.16×10^{-12} s/eV (red dotted). The latter three values are the current results from NOvA, T2K and the combined analysis of these two. It is obvious that for larger neutrino-decay effects, the constraint becomes tighter. The appearance of the upper bound at 3σ, which does not show up in the current measurements, is notable. In the case of $\tau_3/m_3 = 10^{-11}$ s/eV, the lower (upper) bound at 3σ is at $\log_{10}(\tau_3/m_3) \sim -11.25$ (-10.5). With $\tau_3/m_3 = 5.01 \times 10^{-12}$ s/eV, the 3σ constraint is about $10^{-11.5}$–$10^{-11.1}$ s/eV, while with $\tau_3/m_3 = 3.16 \times 10^{-12}$ s/eV the 3σ uncertainty runs from $\sim 10^{-11.65}$ to $\sim 10^{-11.35}$ s/eV. The whole behaviour of $\Delta\chi^2$ is that starting from the true value, it climbs to infinity when τ_3/m_3 gets smaller, while $\Delta\chi^2$ approaches to a certain value when $\tau_3/m_3 \to \infty$. The behaviour can be understood in figures 3 and 4. When τ_3/m_3 is larger enough, the spectra behave the same as those for the stable-neutrino case. Therefore, $\Delta\chi^2$ approaches to a certain value when $\tau_3/m_3 \to \infty$. We note that the behaviour of $\Delta\chi^2$ looks symmetric for $\tau_3/m_3 = 3.16 \times 10^{-12}$ [s/eV] in figure 5, but does not for the larger value of τ_3/m_3. It is because in the case with $\tau_3/m_3 = 3.16 \times 10^{-12}$ [s/eV] $\Delta\chi^2$ is approaching to ~ 120 when $\tau_3/m_3 \to \infty$. The range of $\Delta\chi^2$ shown in figure 5 is near the bottom. Therefore, the behaviour of $\Delta\chi^2$ looks symmetric for $\tau_3/m_3 = 3.16 \times 10^{-12}$ [s/eV].

In figure 6 we compare the result from MOMENT (black curve) with the current experiments (red short-dashed curves), which are taken from ref. [32]. The upper-left panel shows the constraint assuming the case without neutrino decays. As we can see, the bound at 3σ for τ_3/m_3 is pushed up by about one order of magnitude from the bound at

JHEP04(2019)004

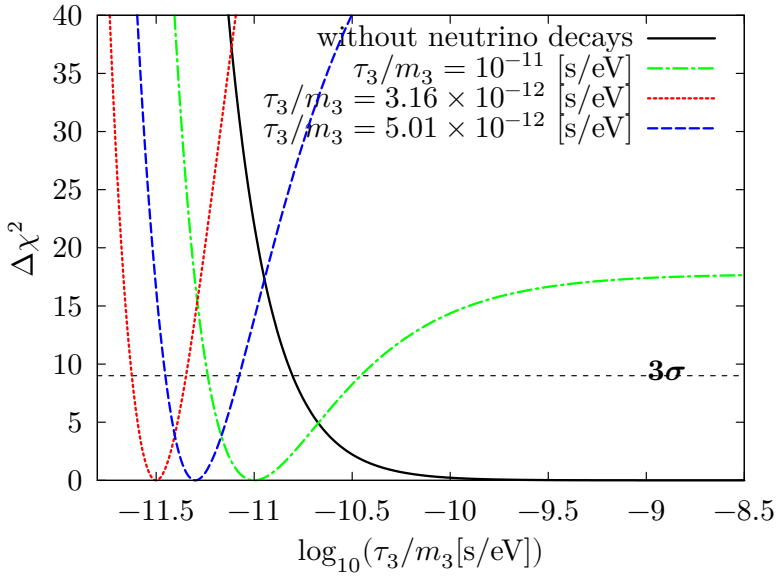

Figure 5. The $\Delta\chi^2 = \chi^2 - \chi^2_{\rm min}$ as a function of the test value of τ_3/m_3 where the input (true) value of τ_3/m_3 is assumed to be ∞ (black solid), 10^{-11} (green dashed-dotted), 5.01×10^{-12} (blue short-dashed) and 3.16×10^{-12} s/eV (red dotted) for MOMENT. We see that as the true value of τ_3/m_3 gets smaller, the constraint becomes tighter, especially the upper bound.

90% C.L. for the combination of T2K and MINOS. Except for the upper left panel, the difference from the curves in figure 5 is that we use the same true values for θ_{23} and Δm^2_{31} as the best fit of ref. [32] in this figure. The most striking feature of MOMENT we see in this figure is that it provides the upper bound for τ_3/m_3 measurement at 3σ, while the lower bound is also greatly reduced. In the other words, instead of giving us a lower bound, MOMENT provides a complete range with the upper and lower limits at a considerable confidence level. The upper bound is important for excluding the case without neutrino decays, if the neutrino decay is confirmed.

From figure 5, it is natural to expect that these experiments have a great ability to exclude the stable-neutrino hypothesis $\tau_3/m_3 = \infty$. We therefore discuss while the true τ_3/m_3 is not infinity, how much MOMENT can exclude the stable-neutrino hypothesis, and therefore find a *hint* of new physics.[1] We show our results in figure 7, in which the red curve is the exclusion ability for MOMENT. The statistical quantity we are studying is $\Delta\chi^2$ for the hypothesis $m_3/\tau_3 = 0$ assuming the various true values τ_3/m_3 (x-axis). We also compare these results with the constraint on τ_3/m_3 assuming the case with neutrino decays (black curves). We find that if in the nature $\log_{10}(\tau_3/m_3[\mathrm{s/eV}]) \sim -10.85$, MOMENT can detect a "*hint*" at around 3σ. These τ_3/m_3 values are larger than our current discovery from T2K and NOvA. This means MOMENT could be sensitive enough to claim a "*hint*" if the current results are confirmed.

[1]We call the tension between the experimental result and the stable-neutrino prediction "*hint*".

JHEP04(2019)004

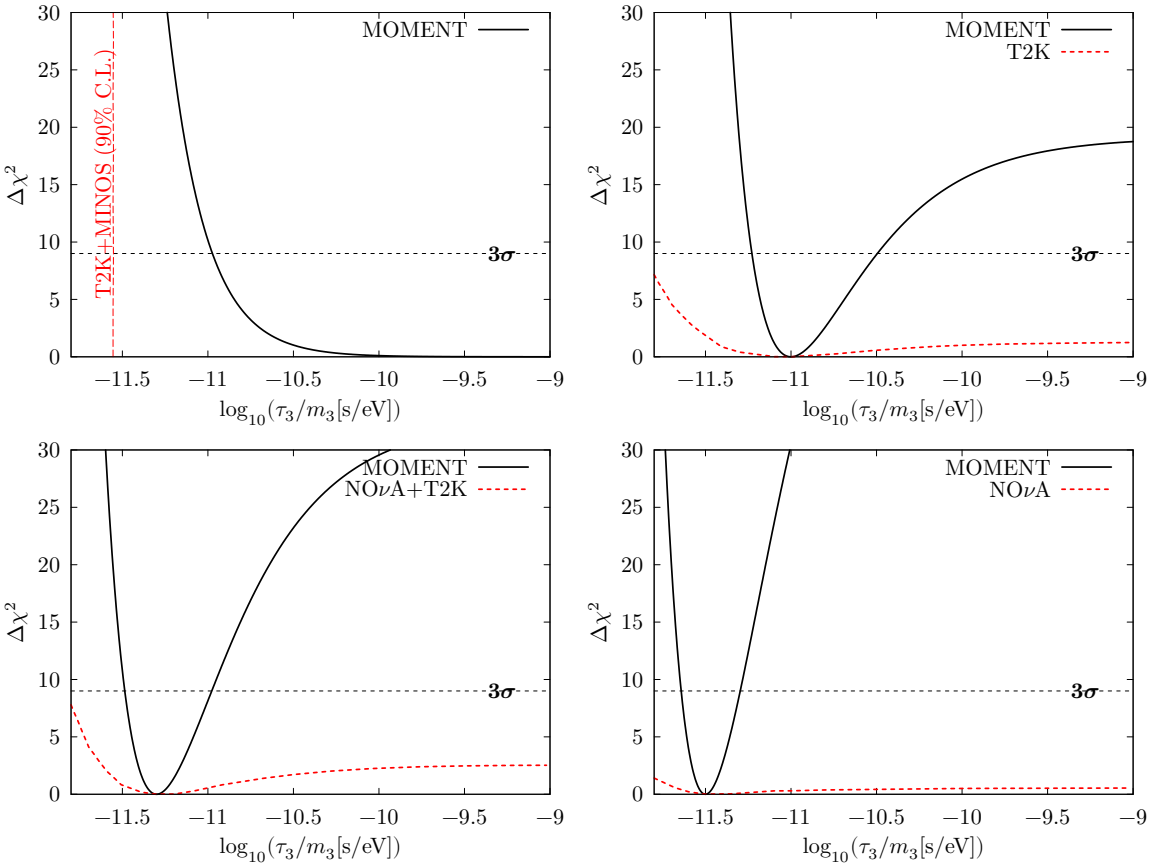

Figure 6. The $\Delta\chi^2 = \chi^2 - \chi^2_{\rm min}$ as a function of the test value of τ_3/m_3 where the inputed true value of τ_3/m_3 is assumed to be ∞ (upper left), 10^{-11} (upper right), 5.01×10^{-12} (lower left) and 3.16×10^{-12} s/eV. The black solid curve is for MOMENT. The short-dashed curves, taken from ref. [32], correspond to current experiments: the upper-left and upper-right panels are the combination of T2K and MINOS and T2K, respectively, while the lower two panel are the combination of T2K and NOvA (left) and NOvA (right).

4.2 Impact of the total running time, systematic uncertainty, and energy resolution

We are interested in studying the impact of the total running time (the short-dashed grey curve), the systematic uncertainty (the black solid curve) and the energy resolution (the red solid curves) in figure 8. We present the constraint power assuming the case without neutrino decays at the 3σ confidence level.[2] Going through the total running time (ν-mode + $\bar{\nu}$-mode) from 1 to 20 years, a 3σ bound can improve from about $\tau_3/m_3 = 10^{-11}$ to $10^{-10.7}$ s/eV. It soars from $\log_{10}(\tau_3/m_3[\mathrm{s/eV}]) = -11$ to about ~ -10.9 at the fourth year before a slow climb to -10.7 at the twentieth year. This means that once it runs for more than 4 years, it gets more difficult to improve the sensitivity by increasing the running time. Moving to the impact of systematic uncertainties, we vary the size of the

[2]We also undergo the same study for the 3σ exclusion ability to the stable-neutrino hypothesis. The results are almost the same as those shown in figure 8.

JHEP04(2019)004

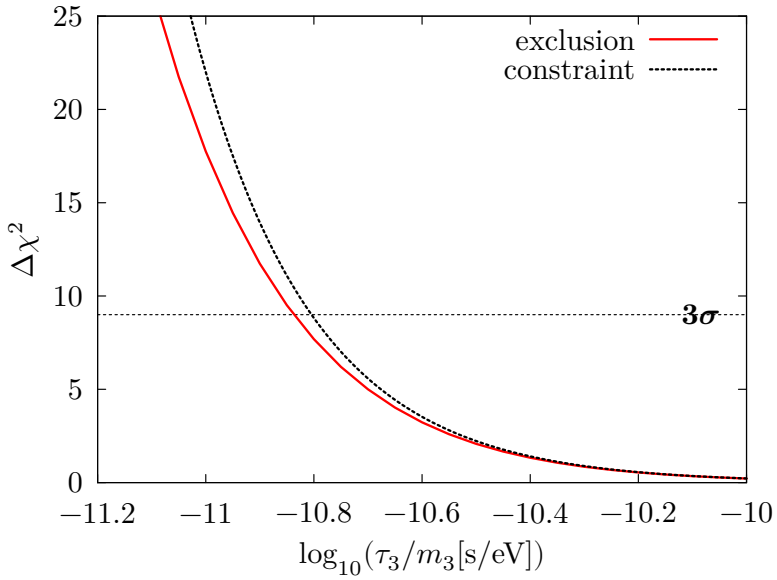

Figure 7. The exclusion ability of the stable-neutrino case $m_3/\tau_3 = 0$ (the red curve) and the constraint on τ_3/m_3 assuming the stable-neutrino case (the black curve). The solid curve corresponds to MOMENT. The exclusion ability is defined as $\Delta\chi^2$ for the hypothesis $m_3/\tau_3 = 0$ for various true values (the x-axis value). We find the exclusion ability could reach 3σ while τ_3/m_3 is below $10^{-10.8}$ s/eV for MOMENT.

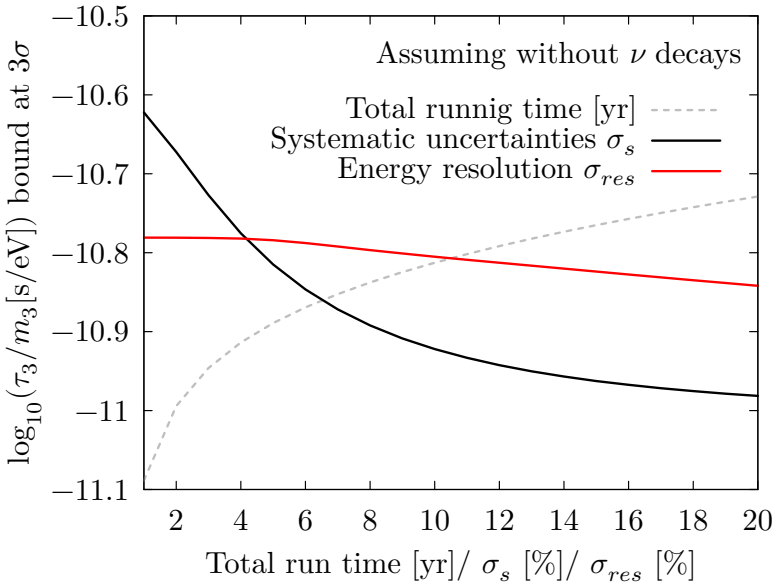

Figure 8. The constraint at 3σ on τ_3/m_3 assuming the stable-neutrino case against the total running time (the short-dashed grey curve), the size of systematic uncertainty σ_s (black), and the energy resolution σ_{res} (red). We focus on the total running time from 1 to 20 years, while σ_s and σ_{res} vary in the range $[1\%, 20\%]$.

JHEP04(2019)004

normalisation uncertainty[3] σ_s from 1 to 20% for all channels. By decreasing σ_s, we can improve the 3σ bound from $\tau_3/m_3 = 10^{-11}$ to $10^{-10.6}$ s/eV. The improvement rises quickly when $\sigma_s < 5\%$ — from $\log_{10}(\tau_3/m_3[\text{s/eV}]) \sim -10.85$ for $\sigma_s = 5\%$ to -10.6 for 1%. Finally, we see relatively small impacts by improving the energy resolution.

We find an important result by comparing two curves, representing the impact of the total running time and σ_s. Our default setting for MOMENT is the case with 10 years for the total running time and roughly the point for $\sigma_s = 5\%$; comparing to two curves, we can see improving $\sigma_s = 1\%$ can improve better ($\log_{10}(\tau_3/m_3[\text{s/eV}]) = -10.6$) than that by doubling the total running time ($\log_{10}(\tau_3/m_3[\text{s/eV}]) = -10.7$). Then, we further conclude that improving our understanding of systematic uncertainties is more important than doubling the total running time.

4.3 Precision measurements of τ_3/m_3 with θ_{23} and Δm^2_{31}

As we see in figure 1, the measurement of τ_3/m_3 largely depends on the disappearance channel, which is sensitive to θ_{23} and Δm^2_{31}. We are therefore interested in the performance of 3σ contours on the $\tau_3/m_3 - \theta_{23}$ (upper-left), $\tau_3/m_3 - \Delta m^2_{31}$ (upper-right) and $\theta_{23} - \Delta m^2_{31}$ (lower) planes in figure 9. We assume three true values: $\tau_3/m_3 = 10^{-11}$ (dashed-dotted green), 5.01×10^{-12} (short-dashed blue) and 3.16×10^{-12} (red dotted) s/eV. Thanks to the high precision of the τ_3/m_3 measurement, we see a complete contour, instead of a band as what we see in current fitting result, shown in ref. [32]. On average, the precision at 3σ of θ_{23} is almost 3–3.5° for MOMENT. We observe some impact from the true τ_3/m_3 value on the θ_{23} measurement. The 3σ uncertainty of Δm^2_{31} is about $0.05 \times 10^{-3}\text{eV}^2$. We further study the 3σ contour on the $\theta_{23} - \Delta m^2_{31}$ plane (the lower panel). We also include results for the stable neutrino case. We consider two scenarios — τ_3/m_3 fixed at ∞ (black) and let this parameter vary (grey). It is obvious that the impact of neutrino decays mainly worsens the measurement of θ_{23} from $\sim 1.5°$ to $\sim$ 3–3.5°. In comparison, there is little impact on the measurement of Δm^2_{31}. We also see a little correlation, once we include τ_3/m_3 into fitting.

5 Summary

In this paper we have considered the third neutrino mass eigenstate ν_3 decaying to invisible states in MOMENT, using eight channels of neutrino oscillation ($\nu_e \to \nu_e$, $\nu_e \to \nu_\mu$, $\nu_\mu \to \nu_e$, $\nu_\mu \to \nu_\mu$ and their CP-conjugate partners) with the help of the following detection processes in a Gd-doped Cherenkov detector: $\nu_e + n \to p + e^-$, $\bar{\nu}_\mu + p \to n + \mu^+$, $\bar{\nu}_e + p \to n + e^+$, and $\nu_\mu + n \to p + \mu^-$. Neutrino decays cause suppression and damping effects on neutrino oscillation probabilities, and could be measured in the reconstructed energy spectra of MOMENT, especially in ν_μ and $\bar{\nu}_\mu$ disappearance channels. And we have found that focusing on the maximum or minimum is a strategy to measure these effects. Events with lower neutrino energy do not only avoid the sizeable matter effect, but also enhance the effects caused by neutrino decays. We have simulated the MOMENT experiment and

[3]The systematic uncertainty, in which we are interested, is the combination of that of fiducial detector volume, flux error for signals, and so on.

JHEP04(2019)004

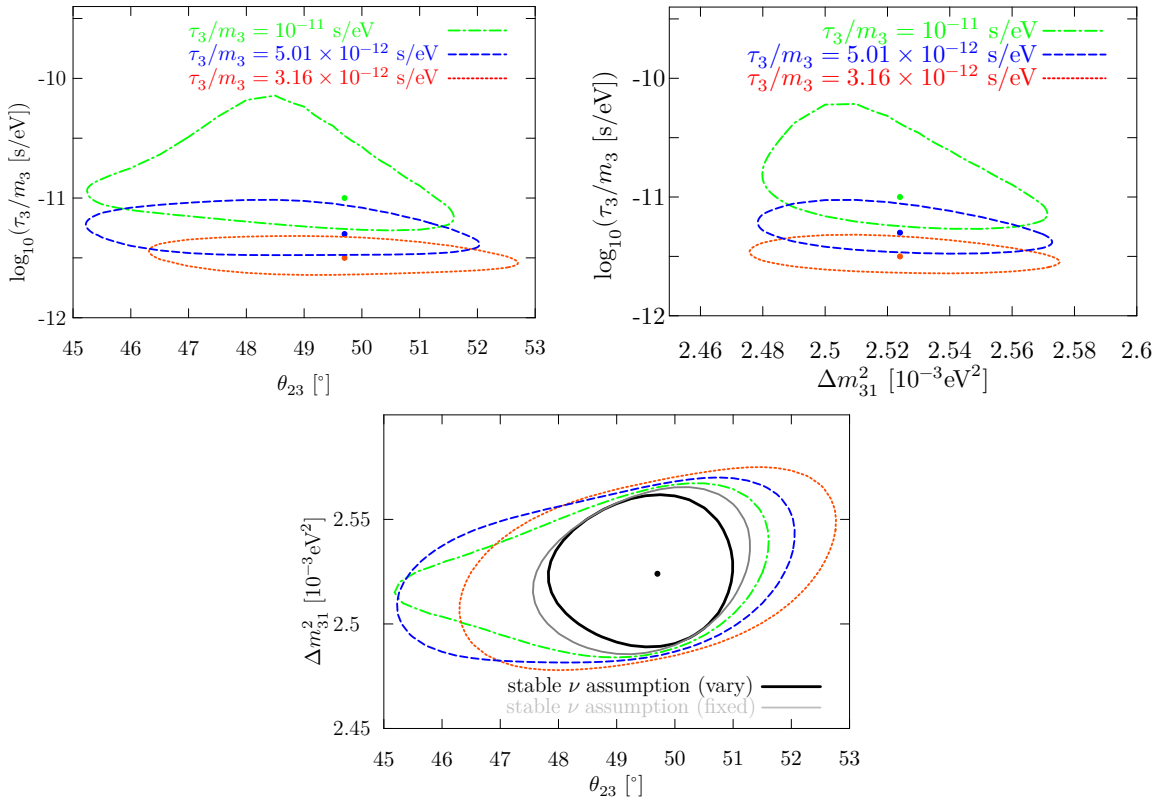

Figure 9. The exclusion contour at 3σ on the planes any two of $\log_{10}(\tau_3/m_3$[s/eV]) and θ_{23} (left) and Δm^2_{31} (right). We show for different true values: $\tau_3/m_3 = 10^{-11}$ (dashed-dotted green), 5.01×10^{-12} (short-dashed blue) and 3.16×10^{-12} (dotted red) s/eV. In the lower panel, we further consider two scenarios — τ_3/m_3 fixed at ∞ (black) and let this parameter vary (grey).

found outstanding potential to constrain the τ_3/m_3 parameter in figure 5. Given the best-fit values hinted by T2K and NOvA [32], we have found that MOMENT would improve the precision measurement of invisible neutrino decays. We reach an interesting conclusion that if the current best fit discovered in [32] is confirmed, the standard non-decay scenario can be excluded with a statistics level higher than 3σ. At 3σ confidence level, the projections of $\theta_{23} - \log_{10}(\tau_3/m_3)$, $\Delta m^2_{31} - \log_{10}(\tau_3/m_3)$ and $\theta_{23} - \Delta m^2_{31}$ have demonstrated little correlations between θ_{23} and Δm^2_{31}. The impact of neutrino decays mainly decrease the 3σ precision of θ_{23} by 1–1.5°.

We have further investigated the impact of statistical and systematic uncertainties by varying the total running time, changing the size of the normalisation uncertainty σ_s and energy resolution respectively. We have demonstrated the 3σ constraint assuming the standard non-decay scenario. By increasing the total running time or reducing the systematic uncertainties, we will improve the sensitivity in invisible neutrino decays. A comparison of two methods has guided us to the conclusion that reducing systematic uncertainties is more important than increasing the total running time in the MOMENT experiment. We have also checked that there is no sizeable impact from improved energy resolution in the detector.

JHEP04(2019)004

As MOMENT has outstanding potential to measure neutrino decays, we also have to emphasize that future atmospheric and astrophysical neutrino experiments will significantly improve the current understanding of neutrino decays. They are complementary to each other, though.

Acknowledgments

This work is supported in part by the National Natural Science Foundation of China under Grant No. 11505301 and No. 11881240247. JT appreciates ICTP's hospitality and scientific activities during the workshop PANE2018. We would like to thank Thomas Hahn for communications and providing a package to diagonize non-hermitain matrices. We would like to thank the accelerator working group of MOMENT for useful discussions and for kindly providing flux files for the MOMENT experiment. Finally, we appreciate Dr. Neil Drouard Raper's help to improve the readability of our paper.

References

[1] SNO collaboration, *Combined Analysis of all Three Phases of Solar Neutrino Data from the Sudbury Neutrino Observatory*, *Phys. Rev.* **C 88** (2013) 025501 [arXiv:1109.0763] [INSPIRE].

[2] Super-Kamiokande collaboration, *Atmospheric neutrino oscillation analysis with sub-leading effects in Super-Kamiokande I, II and III*, *Phys. Rev.* **D 81** (2010) 092004 [arXiv:1002.3471] [INSPIRE].

[3] KamLAND collaboration, *Precision Measurement of Neutrino Oscillation Parameters with KamLAND*, *Phys. Rev. Lett.* **100** (2008) 221803 [arXiv:0801.4589] [INSPIRE].

[4] Daya Bay collaboration, *Measurement of electron antineutrino oscillation based on 1230 days of operation of the Daya Bay experiment*, *Phys. Rev.* **D 95** (2017) 072006 [arXiv:1610.04802] [INSPIRE].

[5] Particle Data Group collaboration, *Review of Particle Physics*, *Chin. Phys.* **C 40** (2016) 100001 [INSPIRE].

[6] I. Esteban, M.C. Gonzalez-Garcia, M. Maltoni, I. Martinez-Soler and T. Schwetz, *Updated fit to three neutrino mixing: exploring the accelerator-reactor complementarity*, *JHEP* **01** (2017) 087 [arXiv:1611.01514] [INSPIRE].

[7] JUNO collaboration, *Status and prospects of the JUNO experiment*, *J. Phys. Conf. Ser.* **888** (2017) 012022 [INSPIRE].

[8] H. Seo, *Status of RENO-50*, PoS(NEUTEL2015)083 (2015).

[9] T2K collaboration, *Neutrino oscillation physics potential of the T2K experiment*, *PTEP* **2015** (2015) 043C01 [arXiv:1409.7469] [INSPIRE].

[10] NOvA collaboration, *First measurement of muon-neutrino disappearance in NOvA*, *Phys. Rev.* **D 93** (2016) 051104 [arXiv:1601.05037] [INSPIRE].

JHEP04(2019)004

[11] DUNE collaboration, *Long-Baseline Neutrino Facility (LBNF) and Deep Underground Neutrino Experiment (DUNE)*, arXiv:1512.06148 [INSPIRE].

[12] T2K collaboration, *Combined Analysis of Neutrino and Antineutrino Oscillations at T2K*, *Phys. Rev. Lett.* **118** (2017) 151801 [arXiv:1701.00432] [INSPIRE].

[13] NOvA collaboration, *Constraints on Oscillation Parameters from ν_e Appearance and ν_μ Disappearance in NOvA*, *Phys. Rev. Lett.* **118** (2017) 231801 [arXiv:1703.03328] [INSPIRE].

[14] A. Acker, S. Pakvasa and J.T. Pantaleone, *Decaying Dirac neutrinos*, *Phys. Rev.* **D 45** (1992) 1 [INSPIRE].

[15] A. Acker and S. Pakvasa, *Solar neutrino decay*, *Phys. Lett.* **B 320** (1994) 320 [hep-ph/9310207] [INSPIRE].

[16] G.B. Gelmini and M. Roncadelli, *Left-Handed Neutrino Mass Scale and Spontaneously Broken Lepton Number*, *Phys. Lett.* **99B** (1981) 411 [INSPIRE].

[17] Y. Chikashige, R.N. Mohapatra and R.D. Peccei, *Are There Real Goldstone Bosons Associated with Broken Lepton Number?*, *Phys. Lett.* **98B** (1981) 265 [INSPIRE].

[18] S. Pakvasa, *Do neutrinos decay?*, *AIP Conf. Proc.* **542** (2000) 99 [hep-ph/0004077] [INSPIRE].

[19] C.W. Kim and W.P. Lam, *Some remarks on neutrino decay via a Nambu-Goldstone boson*, *Mod. Phys. Lett.* **A 5** (1990) 297 [INSPIRE].

[20] A. Acker, A. Joshipura and S. Pakvasa, *A Neutrino decay model, solar anti-neutrinos and atmospheric neutrinos*, *Phys. Lett.* **B 285** (1992) 371 [INSPIRE].

[21] M. Lindner, T. Ohlsson and W. Winter, *A Combined treatment of neutrino decay and neutrino oscillations*, *Nucl. Phys.* **B 607** (2001) 326 [hep-ph/0103170] [INSPIRE].

[22] R. Picoreti, M.M. Guzzo, P.C. de Holanda and O.L.G. Peres, *Neutrino Decay and Solar Neutrino Seasonal Effect*, *Phys. Lett.* **B 761** (2016) 70 [arXiv:1506.08158] [INSPIRE].

[23] J.M. Berryman, A. de Gouvêa and D. Hernandez, *Solar Neutrinos and the Decaying Neutrino Hypothesis*, *Phys. Rev.* **D 92** (2015) 073003 [arXiv:1411.0308] [INSPIRE].

[24] G.-Y. Huang and S. Zhou, *Constraining Neutrino Lifetimes and Magnetic Moments via Solar Neutrinos in the Large Xenon Detectors*, *JCAP* **02** (2019) 024 [arXiv:1810.03877] [INSPIRE].

[25] M.C. Gonzalez-Garcia and M. Maltoni, *Status of Oscillation plus Decay of Atmospheric and Long-Baseline Neutrinos*, *Phys. Lett.* **B 663** (2008) 405 [arXiv:0802.3699] [INSPIRE].

[26] P.B. Denton and I. Tamborra, *Invisible Neutrino Decay Could Resolve IceCube's Track and Cascade Tension*, *Phys. Rev. Lett.* **121** (2018) 121802 [arXiv:1805.05950] [INSPIRE].

[27] P.F. de Salas, S. Pastor, C.A. Ternes, T. Thakore and M. Tórtola, *Constraining the invisible neutrino decay with KM3NeT-ORCA*, *Phys. Lett.* **B 789** (2019) 472 [arXiv:1810.10916] [INSPIRE].

[28] R.A. Gomes, A.L.G. Gomes and O.L.G. Peres, *Constraints on neutrino decay lifetime using long-baseline charged and neutral current data*, *Phys. Lett.* **B 740** (2015) 345 [arXiv:1407.5640] [INSPIRE].

[29] T. Abrahão, H. Minakata, H. Nunokawa and A.A. Quiroga, *Constraint on Neutrino Decay with Medium-Baseline Reactor Neutrino Oscillation Experiments*, *JHEP* **11** (2015) 001 [arXiv:1506.02314] [INSPIRE].

JHEP04(2019)004

[30] S. Choubey, S. Goswami, C. Gupta, S.M. Lakshmi and T. Thakore, *Sensitivity to neutrino decay with atmospheric neutrinos at the INO-ICAL detector*, *Phys. Rev.* **D 97** (2018) 033005 [arXiv:1709.10376] [INSPIRE].

[31] S. Choubey, S. Goswami and D. Pramanik, *A study of invisible neutrino decay at DUNE and its effects on θ_{23} measurement*, *JHEP* **02** (2018) 055 [arXiv:1705.05820] [INSPIRE].

[32] S. Choubey, D. Dutta and D. Pramanik, *Invisible neutrino decay in the light of NOvA and T2K data*, *JHEP* **08** (2018) 141 [arXiv:1805.01848] [INSPIRE].

[33] A.M. Gago, R.A. Gomes, A.L.G. Gomes, J. Jones-Perez and O.L.G. Peres, *Visible neutrino decay in the light of appearance and disappearance long baseline experiments*, *JHEP* **11** (2017) 022 [arXiv:1705.03074] [INSPIRE].

[34] A.G. Doroshkevich and M.Y. Khlopov, *Formation of structure in the Universe with unstable neutrinos*, *Mon. Not. Roy. Astron. Soc.* **211** (1984) 277.

[35] A.G. Doroshkevich, M. Khlopov and A.A. Klypin, *Large-scale structure of the universe in unstable dark matter models*, *Mon. Not. Roy. Astron. Soc.* **239** (1989) 923 [INSPIRE].

[36] J. Cao et al., *Muon-decay medium-baseline neutrino beam facility*, *Phys. Rev. ST Accel. Beams* **17** (2014) 090101 [arXiv:1401.8125] [INSPIRE].

[37] M.B. Gavela, D. Hernandez, T. Ota and W. Winter, *Large gauge invariant non-standard neutrino interactions*, *Phys. Rev.* **D 79** (2009) 013007 [arXiv:0809.3451] [INSPIRE].

[38] F. Bonnet, D. Hernandez, T. Ota and W. Winter, *Neutrino masses from higher than $d = 5$ effective operators*, *JHEP* **10** (2009) 076 [arXiv:0907.3143] [INSPIRE].

[39] M.B. Krauss, T. Ota, W. Porod and W. Winter, *Neutrino mass from higher than $d = 5$ effective operators in SUSY and its test at the LHC*, *Phys. Rev.* **D 84** (2011) 115023 [arXiv:1109.4636] [INSPIRE].

[40] S. Gariazzo, C. Giunti, M. Laveder and Y.F. Li, *Updated Global 3+1 Analysis of Short-BaseLine Neutrino Oscillations*, *JHEP* **06** (2017) 135 [arXiv:1703.00860] [INSPIRE].

[41] K.N. Abazajian et al., *Light Sterile Neutrinos: A White Paper*, arXiv:1204.5379 [INSPIRE].

[42] M. Drewes et al., *A White Paper on keV Sterile Neutrino Dark Matter*, *JCAP* **01** (2017) 025 [arXiv:1602.04816] [INSPIRE].

[43] P. Minkowski, *$\mu \to e\gamma$ at a Rate of One Out of 10^9 Muon Decays?*, *Phys. Lett.* **67B** (1977) 421 [INSPIRE].

[44] MiniBooNE collaboration, *Significant Excess of ElectronLike Events in the MiniBooNE Short-Baseline Neutrino Experiment*, *Phys. Rev. Lett.* **121** (2018) 221801 [arXiv:1805.12028] [INSPIRE].

[45] Z. Maki, M. Nakagawa and S. Sakata, *Remarks on the unified model of elementary particles*, *Prog. Theor. Phys.* **28** (1962) 870 [INSPIRE].

[46] B. Pontecorvo, *Mesonium and anti-mesonium*, *Sov. Phys. JETP* **6** (1957) 429 [INSPIRE].

[47] T. Hahn, *Routines for the diagonalization of complex matrices*, physics/0607103 [INSPIRE].

[48] J. Tang and Y. Zhang, *Study of nonstandard charged-current interactions at the MOMENT experiment*, *Phys. Rev.* **D 97** (2018) 035018 [arXiv:1705.09500] [INSPIRE].

[49] J. Tang, Y. Zhang and Y.-F. Li, *Probing Direct and Indirect Unitarity Violation in Future Accelerator Neutrino Facilities*, *Phys. Lett.* **B 774** (2017) 217 [arXiv:1708.04909] [INSPIRE].

JHEP04(2019)004

[50] J.-E. Campagne, M. Maltoni, M. Mezzetto and T. Schwetz, *Physics potential of the CERN-MEMPHYS neutrino oscillation project*, *JHEP* **04** (2007) 003 [hep-ph/0603172] [INSPIRE].

[51] HYPER-KAMIOKANDE WORKING GROUP collaboration, *T2HK: J-PARC upgrade plan for future and beyond T2K*, in *15th International Workshop on Neutrino Factories, Super Beams and Beta Beams (NuFact2013)*, Beijing, China, August 19–24, 2013 (2013) [arXiv:1311.5287] [INSPIRE].

[52] P. Huber, M. Lindner and W. Winter, *Simulation of long-baseline neutrino oscillation experiments with GLoBES (General Long Baseline Experiment Simulator)*, *Comput. Phys. Commun.* **167** (2005) 195 [hep-ph/0407333] [INSPIRE].

[53] P. Huber, J. Kopp, M. Lindner, M. Rolinec and W. Winter, *New features in the simulation of neutrino oscillation experiments with GLoBES 3.0: General Long Baseline Experiment Simulator*, *Comput. Phys. Commun.* **177** (2007) 432 [hep-ph/0701187] [INSPIRE].

JHEP04(2019)004